Journal of Power Sources 285 (2015) 156–160

Contents lists available at ScienceDirect

Journal of Power Sources

journal homepage: www.elsevier.com/locate/jpowsour

Deciphering the thermal behavior of lithium rich cathode material by *in situ* X-ray diffraction technique

Shoaib Muhammad [a, 1], Sangwoo Lee [a, 1], Hyunchul Kim [a], Jeongbae Yoon [a], Donghyuk Jang [a], Jaegu Yoon [b], Jin-Hwan Park [b], Won-Sub Yoon [a, *]

[a] Department of Energy Science, Sungkyunkwan University, Suwon 440-746, South Korea
[b] Energy Lab, Samsung Advanced Institute of Technology, Suwon 443-803, South Korea

HIGHLIGHTS

- Thermal degradation mechanism of lithium rich electrode material is investigated.
- In the absence of electrolyte, LMC shows better thermal stability compared to NMC.
- In the presence of electrolyte, thermal decomposition of LMC is accelerated.
- Catalytic activity of electrolyte in thermal decomposition is electrode dependent.

GRAPHICAL ABSTRACT

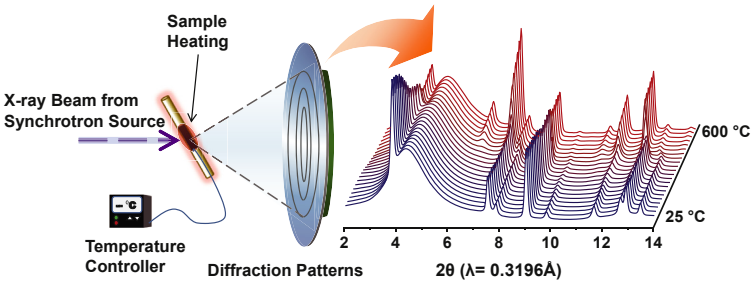

ARTICLE INFO

Article history:
Received 19 November 2014
Received in revised form
5 February 2015
Accepted 8 March 2015
Available online 14 March 2015

Keywords:
In situ X-ray diffraction
Thermal stability
Lithium rich cathode material
Lithium-ion battery

ABSTRACT

Thermal stability is one of the critical requirements for commercial operation of high energy lithium-ion batteries. In this study, we use *in situ* X-ray diffraction technique to elucidate the thermal degradation mechanism of $0.5Li_2MnO_3$-$0.5LiNi_{0.33}Co_{0.33}Mn_{0.33}O_2$ lithium rich cathode material in the absence and presence of electrolyte to simulate the real life battery conditions and compare its thermal behavior with the commercial $LiNi_{0.33}Co_{0.33}Mn_{0.33}O_2$ cathode material. We show that the thermal induced phase transformations in delithiated lithium rich cathode material are much more intense compared to similar single phase layered cathode material in the presence of electrolyte. The structural changes in both cathode materials with the temperature rise follow different trends in the absence and presence of electrolyte between 25 and 600 °C. Phase transitions are comparatively simple in the absence of electrolyte, the fully charged lithium rich cathode material demonstrates better thermal stability by maintaining its phase till 379 °C, and afterwards spinel structure is formed. In the presence of electrolyte, however, the spinel structure appears at 207 °C, subsequently it transforms to rock salt type cubic phase at 425 °C with additional metallic, metal fluoride, and metal carbonate phases.

1. Introduction

Lithium-ion batteries were introduced in 1990 by Sony Corporation. Since its successful debut, various transition metal oxides have been synthesized and investigated as new lithium ion battery electrode materials to fulfill the ever demanding high capacity requirements. Recently composite layered material between Li_2MnO_3

* Corresponding author. Department of Energy Science, Sungkyunkwan University. Natural Sciences Campus, 2066, Seobu-ro, Jangan-gu, Suwon-si, Gyeonggi-do, 440-746, South Korea.
E-mail address: wsyoon@skku.edu (W.-S. Yoon).
[1] These authors equally contributed to this work.

http://dx.doi.org/10.1016/j.jpowsour.2015.03.054
0378-7753/

and $LiMO_2$ (where M = Mn, Co, Ni), also known as the lithium rich cathode material, has received pronounced attention and has been considered as promising cathode material due to its high discharge capacity of ~250 mAh g^{-1} [1]. However, there are several intrinsic problems associated with this material family that need to be solved; e.g., the voltage as well as the capacity decay during cycling, the high irreversible capacity loss in the first cycle, poor rate capability, and oxygen release during cycling, in order to adopt these materials in practical cells [2–4]. Thermal stability is another challenge which could greatly impact the safety of lithium-ion batteries, however it has received little attention unlike the widely studied electrochemical performance and reaction mechanism of this material.

In this study, we synthesized $0.5Li_2MnO_3$-$0.5LiNi_{0.33}Co_{0.33}Mn_{0.33}O_2$ (LMC) and applied the *in situ* XRD to monitor the in depth thermal behavior of this cathode material in the presence and absence of electrolyte as a function of temperature. XRD is a powerful technique to study the crystal structure and can provide the roadmap on average bulk structural changes during thermal decomposition, which is crucial to understand the thermal behavior of electrode materials [5–7]. Utilization of this technique during heating the electrode materials in the presence of electrolyte can simulate the real life battery conditions and provides meaningful information about the thermal decomposition of the electrode materials. In our previous studies, we have successfully employed this technique to study the thermal degradation mechanism of nickel-based cathode materials [8–12]. Monoclinic Li_2MnO_3 phase in a lithium rich cathode material acts as additional lithium sources and provides the anomalous high capacity when lithium rich cathode material is cycled above 4.4 V. In order to evaluate the impact of Li_2MnO_3 on the thermal stability of this cathode material, thermal induced phase transitions of this selected lithium rich cathode material were comparatively studied with the commercial $LiNi_{0.33}Co_{0.33}Mn_{0.33}O_2$ cathode material, also known as NCM. Outcomes of this study furnish the fundamental understanding of phase transitions in lithium rich cathode material under the thermal abuse and provide guidelines for further research and development in this material for commercial applications.

2. Experimental

$0.5Li_2MnO_3$-$0.5LiNi_{0.33}Co_{0.33}Mn_{0.33}O_2$ powder was synthesized by a sol–gel method [13]. 0.05 mol of lithium acetate $Li(CH_3COO).2H_2O$ and stoichiometric amounts of nickel acetate $Ni(CH_3COO)_2.4H_2O$, cobalt nitrate $Co(NO_3)_2.6H_2O$, and manganese acetate $Mn(CH_3COO)_2.4H_2O$ were dissolved in 190 ml distilled water. The mixed metal solution was added drop-wise to aqueous solution of 10 ml (60%) nitric acid HNO_3, 15 ml of citric acid $C_6H_8O_7$, and 15 ml of ethylene glycol $C_2H_6O_2$ with constant stirring. The pH of the resulting solution was adjusted to 7.5 using ammonium hydroxide before solvent evaporation to get a transparent viscous gel. This gel was calcined at 950 °C for 5 h in air to obtain the desired cathode material.

High resolution synchrotron X-ray powder diffraction (HRPD) measurements of the synthesized $0.5Li_2MnO_3$-$0.5LiNi_{0.33}Co_{0.33}Mn_{0.33}O_2$ powder were carried out at 9B HRPD beam line at Pohang Light Source-II in South Korea. The pristine powder sample was scanned from 10 to 130.5° with step size of 0.01°. The incident X-rays were vertically collimated using a mirror and monochromatized to wavelength of 1.5475 Å using a double-crystal Si (111) monochromator. The detector arm of diffractometer consisted of soller slits with an angular resolution of 2°, a flat Ge (111) crystal analyzer, an antiscatter baffle, and a scintillation detector.

The electrodes were prepared by mixing 8 wt% PVDF (Kureha) and 8 wt% carbon black (Chevron) in synthesized cathode material to prepare the slurry. The electrode films were formed on Al foil current collector by slurry coating technique. 2032-type coin cells were assembled in the dry room by using Celgard separator, lithium foil as counter electrode, and 1.3 M $LiPF_6$ electrolyte dissolved in ethylene carbonate/dimethyl carbonate (3:7 by volume) solvent. The cells were fully charged at low current rate of 0.05C to cut-off voltage of 4.7 V using constant current and constant voltage mode, and the net charge capacity of 311 mAh g^{-1} was achieved. The electrode material was scratched from the current collector and loaded into quartz capillaries whereas for the electrolyte-free samples, charged electrodes were washed with excess dimethyl carbonate in the glove box. For the electrolyte containing, a drop excess electrolyte was added in the capillaries after the samples were washed and loaded. The capillaries were sealed in glove box before mounting on the thermal stage of the diffract-photometer of beamline X7B at National Synchrotron Light Source, Brookhaven National Laboratory. The wavelength used at X7B was 0.3196 Å. The spectra were recorded as a set of circles on Mar 345-image plate detector in transmission mode for ~1 min of exposure time while temperature was raised at the rate of 2.5 °C min^{-1}. In order to make an easy comparison with the results in the literature, all the 2θ angles in this paper have been converted to the values corresponding to the CuKα radiation (λ = 1.54056 Å). Rietveld refinement of recorded HRPD pattern and Pawley fitting of *in situ* XRD patterns were performed by using GSAS-II package [14].

3. Results and discussion

High resolution powder diffraction pattern and Rietveld refined fit of the synthesized $0.5Li_2MnO_3$-$0.5LiNi_{0.33}Co_{0.33}Mn_{0.33}O_2$ powder are shown in Fig. 1, and detailed structural parameters are tabulated in Table 1. Most of the peaks in the pattern were indexed based on a hexagonal α-$NaFeO_2$ type structure with *R-3m* space group. The weak peaks between 20 and 30° are originated from monoclinic Li_2MnO_3-like *C2/m* super lattice, caused by local ordering of Li and Mn in the transition metal layers [15]. Clear splitting of the (006)/(102) and (108)/(110) reflection pairs indicates a well-defined hexagonal structure [16]. Excellent agreement between observed and calculated pattern in Rietveld fit shows that the desired lithium rich composition was successfully synthesized. *In situ* XRD patterns of the fully charged $0.5Li_2MnO_3$-0.5 $LiNi_{0.33}Co_{0.33}Mn_{0.33}O_2$ and $LiNi_{0.33}Co_{0.33}Mn_{0.33}O_2$ cathode materials during heating from 25 to 600 °C in the absence of electrolyte are shown in Fig. 2. XRD patterns for charged $LiNi_{0.33}Co_{0.33}Mn_{0.33}O_2$ were obtained by

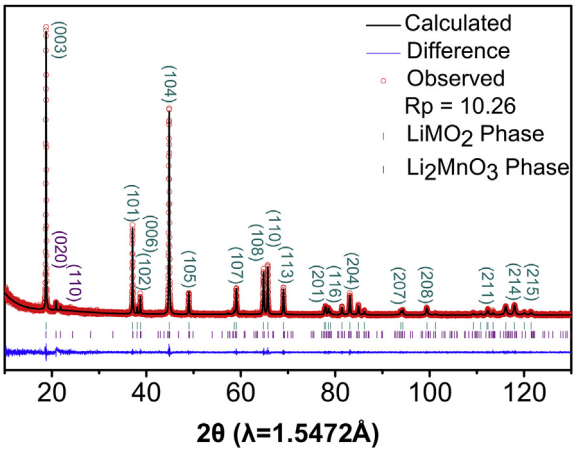

Fig. 1. The Rietveld refined fit of $0.5Li_2MnO_3$-$0.5LiMn_{0.33}Co_{0.33}Ni_{0.33}O_2$ pristine powder HRPD spectrum.

Table 1
The Rietveld refined structural parameters of pristine $0.5Li_2MnO_3$-$0.5LiNi_{0.33}Co_{0.33}Mn_{0.33}O_2$ cathode powder.

Composition (space group)	Site	Atom	Atomic coordinates			U_{ISO}	Occ.	Lattice parameters
			x	y	z			
$LiNi_{0.33}Mn_{0.33}Co_{0.33}O_2$ *(R-3m)*	3b	Li	0	0	0.5	0.0094	0.98	a, b = 2.851 Å
	3b	Ni	0	0	0.5	0.0094	0.02	c = 14.231 Å
	3a	Ni	0	0	0	0.0015	0.31	α, β = 90°
	3a	Co	0	0	0	0.0015	0.33	γ = 120°
	3a	Mn	0	0	0	0.0015	0.33	
	6c	O	0	0	0.258	0.0029	1.0	
Li_2MnO_3 *(C2/m)*	2b	Li	0	0.5	0	0.0100	1.0	a = 4.931 Å
	2c	Li	0	0	0.5	0.1200	1.0	b = 8.542 Å
	4h	Li	0	0.737	0.5	0.1700	1.0	c = 5.035 Å
	4g	Mn	0	0.167	0	0.0295	1.0	α = 90°
	4i	O	0.235	0	0.225	0.0666	1.0	β = 109.33°
	8j	O	0.244	0.323	0.229	0.0662	1.0	γ = 90°

replotting our previously published data for comparison purpose [9]. At 25 °C, XRD patterns of both the cathode materials can be indexed as hexagonal structure with *R-3m* space group. A closer look at Fig. 2 reveals that the intensity ratio of (003)/(104) reflections in rhombohedral structures start to decrease by increasing the temperature. The integrated intensity ratio of (003)/(104) depends on degree of displacement between the transition metals and lithium ions at 3a and 3b sites respectively in *R-3m* space group. Therefore, the decrease in (003)/(104) intensity ratio indicates increase in cation disorder by increasing the temperature [17]. The distorted oxygen sub lattice in hexagonal α-$NaFeO_2$ structure gives rise to clear splitting of (108) and (110) reflections. These two reflections merge together when there is no distortion in the c direction, and structure is totally cubic [18]. By increasing temperature (108) and (110), reflections merge into (440) reflection, indicating the conversion of hexagonal to cubic spinel phase at ~379 °C for $0.5Li_2MnO_3$-$0.5LiNi_{0.33}Co_{0.33}Mn_{0.33}O_2$ and ~350 °C for $LiNi_{0.33}Co_{0.33}Mn_{0.33}O_2$. The lithium rich cathode material exhibits better thermal stability than the NCM in the absence of electrolyte. This behavior can be attributed to the strong octahedral site preference of manganese. Both hexagonal and spinel structures are based on the cubic close packed frame work of oxygen atoms. In hexagonal *R-3m* type structure, lithium and transition metal ions occupy alternating octahedral sites, whereas in cubic spinel *Fd-3m* type structure, the lithium ions take the 8a tetrahedral, and the transition metal occupy the 16d octahedral sites. In order for hexagonal structure to transform into cubic spinel type structure, the transition metal must hop through the neighboring tetrahedral site to reach next octahedral site and theoretical calculations show that activation barrier for Mn^{4+} octahedron-tetrahedron hop is significantly higher than that of cobalt [19]. The lithium rich cathode material has additional Mn^{4+} content because of its Li_2MnO_3 phase compared to bare $LiNi_{0.33}Co_{0.33}Mn_{0.33}O_2$, which will impede its hexagonal to cubic spinel phase transition. Upon further heating, the formed spinel structure undergoes another phase transition, as indicated by the appearance and the gradual increase of the (220) and (422) reflections intensities. These reflections are due to the increased partial occupancy of transition metal at the tetrahedral 8a site, and the appearance of these new reflections means that upon further heating both the cathode materials transform to M_3O_4-type *Fd-3m* spinel structure [20].

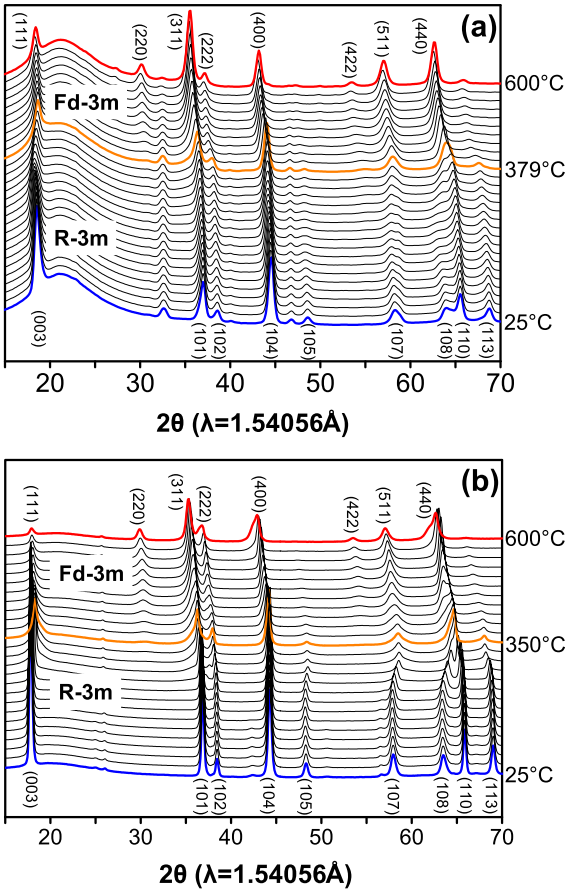

Fig. 2. *In situ* X-ray diffraction patterns of charged (a) $0.5Li_2MnO_3$-$0.5LiMn_{0.33}Co_{0.33}Ni_{0.33}O_2$ and (b) $LiMn_{0.33}Co_{0.33}Ni_{0.33}O_2$ cathode material during heating from 25 to 600 °C in the absence of electrolyte.

In situ XRD patterns of charged $0.5Li_2MnO_3$-$0.5LiNi_{0.33}Co_{0.33}Mn_{0.33}O_2$ and $LiNi_{0.33}Co_{0.33}Mn_{0.33}O_2$ cathode materials during heating from 25 to 600 °C in the presence of electrolyte are shown in Fig. 3. At 25 °C, the XRD patterns of both electrodes can be indexed as hexagonal structure with *R-3m* space group. By increasing temperature, the hexagonal phase converts to the cubic spinel phase at ~207 °C for $0.5Li_2MnO_3$-0.5 $LiNi_{0.33}Co_{0.33}Mn_{0.33}O_2$ and ~304 °C for $LiNi_{0.33}Co_{0.33}Mn_{0.33}O_2$. These temperatures are significantly lower than the onset temperatures of similar phase transitions in the absence of electrolyte. Upon further heating, series of drastic phase transitions take place, and the charged cathode material transforms to the rock salt type cubic structure with *Fm3m* space group at ~422 °C for $0.5Li_2MnO_3$-$0.5LiNi_{0.33}Co_{0.33}Mn_{0.33}O_2$ and ~441 °C for $LiNi_{0.33}Co_{0.33}Mn_{0.33}O_2$ with a secondary metallic phase, and the quantity of metallic phase increases by further increasing the temperature up to 600 °C. Hexagonal *R-3m* to cubic *Fd-3m* structure conversion involves movement of transition metals from a near perfect layered arrangement of lithium and

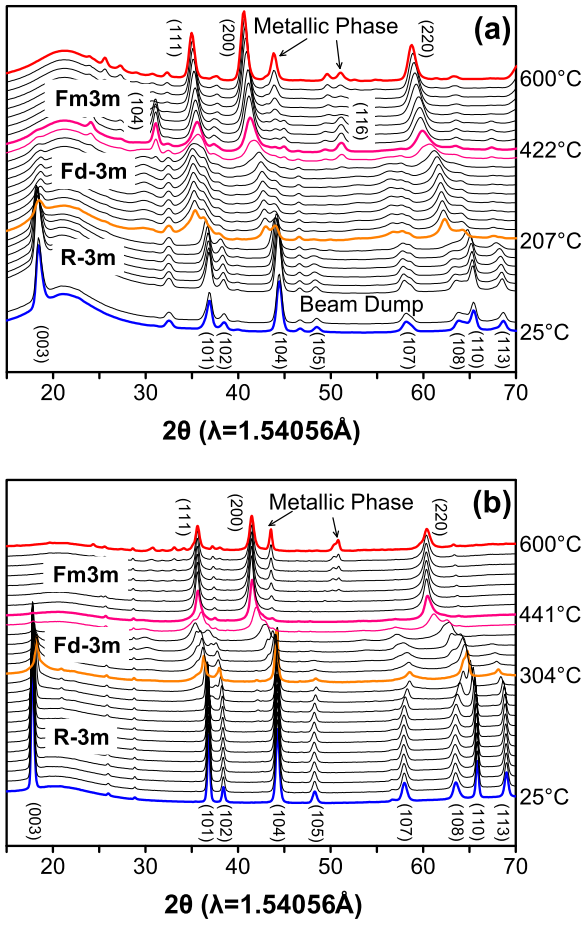

Fig. 3. *In situ* X-ray diffraction patterns of charged (a) $0.5Li_2MnO_3$-$0.5LiMn_{0.33}Co_{0.33}Ni_{0.33}O_2$ and (b) $LiMn_{0.33}Co_{0.33}Ni_{0.33}O_2$ cathode material during heating from 25 to 600 °C in the presence of electrolyte.

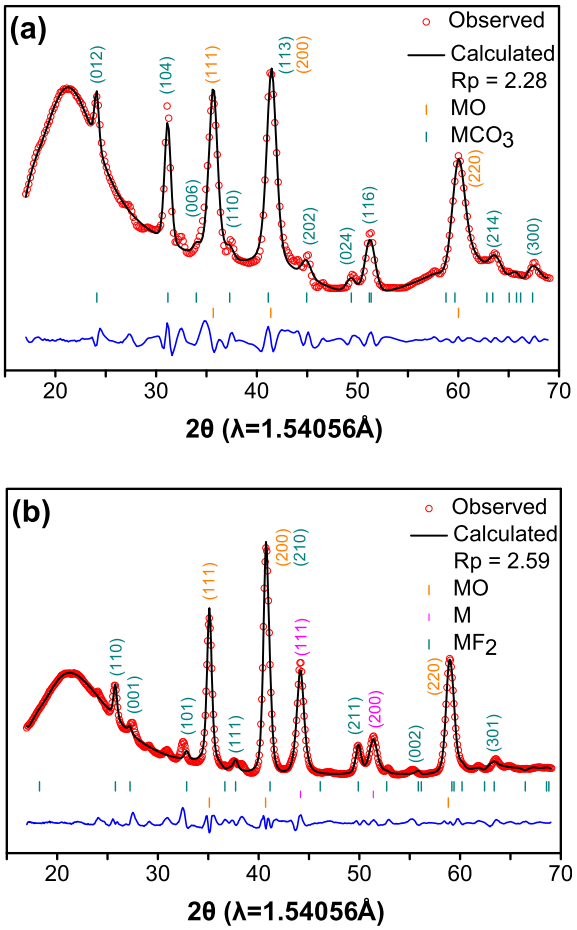

Fig. 4. The Pawley fit of selected *in situ* X-ray diffraction patterns of charged $0.5Li_2MnO_3$-$0.5LiMn_{0.33}Co_{0.33}Ni_{0.33}O_2$ cathode material at (a) 422 °C and (b) 600 °C in the presence of electrolyte.

transition metal to the 1/4th occupancy of transition metal in the lithium layer [21]. Increasing the temperature in the presence of electrolyte enhances the movement of transition metals, and the structure becomes rock salt when transition metal ions are randomly distributed in each octahedral layer [5]. Interestingly the prominent reflections for M_3O_4-type spinel phase were not observed in the presence of electrolyte, likely due to faster kinetics of thermal degradation reaction in the presence of electrolyte. In the case of the lithium rich cathode material, a few additional phases can be observed at high temperature. To index these additional unknown phases and further analyze the thermally induced phase evolution in $0.5Li_2MnO_3$-$0.5LiNi_{0.33}Co_{0.33}Mn_{0.33}O_2$ in the presence of electrolyte, Pawley fitting of diffraction patterns at selected temperatures of ~422 and ~600 °C was performed as shown in Fig. 4 [22]. Pawley fitting is a natural choice for the fitting of these *in situ* diffraction patterns over Rietveld method since perfect crystalline phases cannot be expected during heating of sample. Fitting of diffraction pattern recorded at 422 °C shows the presence of metal carbonate *R-3c* type hexagonal phase (JCPDS 44-1472) along with the main rock salt MO-type phase. At least two more phases' namely cubic pure metallic and rutile type metal fluoride (JCPDS 1-601) can be distinguished at terminal temperature along with the MO-type rock salt phase. These new phases are formed by the combination of decomposed electrolyte products with cathode material at higher temperature. Electrolyte used in lithium ion batteries contains $LiPF_6$ salt dissolved in ethyl and ethyl methyl carbonate solvents. $LiPF_6$ is known to decompose as: $LiPF_6 \rightarrow LiF + PF_5$ [23]. PF_5 is a strong Lewis acid which can result in ring opening of ethyl carbonate solvent. PF_5 can also react with trace water in the electrolyte to form HF which leads to solvent decomposition. Decomposition of electrolyte solvents result in different gaseous species including CO_2, C_2H_4, and C_2H_5F [24]. These electrolyte decomposition products then attack the electrode material at high temperature to form metal carbonates and metal fluorides phases along with catalyzing the thermal decomposition of electrode material. Lithium rich cathode material is notorious for releasing the oxygen in the first charge and contains defect sites in fully charged state [25]. These defects may act as nucleation sites of new phases in the presence of electrolyte at high temperature [26]. The appearance of these additional new phases in the charged lithium rich cathode material indicates that lithium rich cathode material is much more sensitive to the thermal decomposition reaction with electrolyte as compared to other nickel-based layered cathode materials.

Schematic illustration of phase transformations in charged $0.5Li_2MnO_3$-$0.5LiNi_{0.33}Co_{0.33}Mn_{0.33}O_2$ as a function of temperature in the presence and absence of electrolyte is shown in Fig. 5. Lithium rich cathode transforms to spinel phase at higher temperature in the absence of electrolyte, and this phase coexists with M_3O_4-type spinel till 600 °C. In the presence of electrolyte, the hexagonal structure converts to disordered spinel at ~207 °C and coexists with negligible quantity of M_3O_4-type spinel till ~422 °C where a metal carbonate phase appears due to active participation

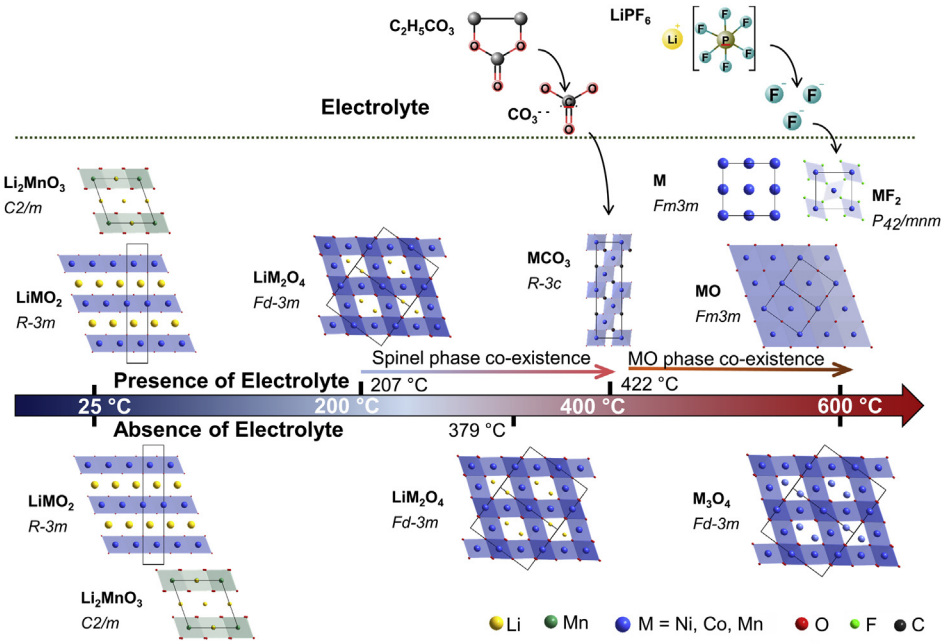

Fig. 5. Schematic illustration of structural changes of charged $0.5Li_2MnO_3$-$0.5LiMn_{0.33}Co_{0.33}Ni_{0.33}O_2$ during heating from 25 to 600 °C in the absence and presence of electrolyte.

of the decomposed electrolyte products in the thermal degradation reaction of lithium rich cathode material, and spinel phase transforms to cubic rock salt MO-type structure with *Fm3m* space group. By heating up to 600 type °C, further phase transitions take place, metal carbonate MCO_3 phase disappears, and new metal fluoride along with pure metallic phases emerge along with previously formed MO-type phase.

4. Conclusions

Lithium rich cathode material $0.5Li_2MnO_3$-$0.5LiNi_{0.33}Co_{0.33}Mn_{0.33}O_2$ was successfully synthesized by the sol–gel method. Thermal stability and structural changes of this cathode material were studied by using synchrotron-based *in situ* XRD technique during raising the electrode temperature. In the absence of electrolyte, phase transitions were simple and limited to spinel structure till the termination temperature of 600 °C without any secondary phase. However, in the presence of electrolyte, structural changes started at relatively lower onset temperatures, the layered structure transformed to spinel followed by a rock salt and pure metallic structure. Metal carbonate and metal fluoride structures also appeared at ~422 and ~600 °C respectively in the lithium rich cathode material due to the reaction of decomposed electrolyte products with cathode material. These results suggest that the presence of electrolyte assists the structural changes at comparatively lower temperatures, and the catalytic activity of electrolyte varies for different electrode materials. The lithium rich cathode material demonstrated better thermal stability in the absence of electrolyte owing to its additional Mn^{4+} content. However, it exhibited thermal instability towards electrolyte in electrochemically delithiated state due to the presence of defect sites after activation of Li_2MnO_3 domain. The findings of this study provide crucial information about thermal behavior of the lithium rich cathode material and help design safer high energy lithium ion batteries.

Acknowledgments

This work was supported by the Fundamental R&D Program for Technology of World Premier Materials and Energy Efficiency & Resources (2010T100200295) of Ministry of Knowledge Economy. This work was also supported by the Human Resources development program (No.20124010203270) of KETEP funded by the Korean government Ministry of Knowledge Economy.

References

[1] M.M. Thackeray, S.-H. Kang, C.S. Johnson, J.T. Vaughey, R. Benedek, S.A. Hackney, J. Mater. Chem. 17 (2007) 3112.
[2] Y. Li, M. Bettge, B. Polzin, Y. Zhu, M. Balasubramanian, D.P. Abraham, J. Electrochem. Soc. 160 (2013) A3006.
[3] A.R. Armstrong, M. Holzapfel, P. Novák, C.S. Johnson, S.-H. Kang, M.M. Thackeray, P.G. Bruce, J. Am. Chem. Soc. 128 (2006) 8694.
[4] X. Yu, Y. Lyu, L. Gu, H. Wu, S.-M. Bak, Y. Zhou, K. Amine, S.N. Ehrlich, H. Li, K.-W. Nam, X.-Q. Yang, Adv. Energy Mater. 4 (2014) 1614.
[5] K.-K. Lee, W.-S. Yoon, K.-B. Kim, K.-Y. Lee, S.-T. Hong, J. Power Sources 97–98 (2001) 321.
[6] K.-K. Lee, W.-S. Yoon, K.-B. Kim, J. Electrochem. Soc. 148 (2001) A1164.
[7] K.-K. Lee, W.-S. Yoon, K.-B. Kim, K.-Y. Lee, S.-T. Hong, J. Electrochem. Soc. 148 (2001) A716.
[8] Y.-H. Cho, D. Jang, J. Yoon, H. Kim, T.K. Ahn, K.-W. Nam, Y.-E. Sung, W.-S. Kim, Y.-S. Lee, X.-Q. Yang, W.-S. Yoon, J. Alloys Compd. 562 (2013) 219.
[9] K.-W. Nam, W.-S. Yoon, X.-Q. Yang, J. Power Sources 189 (2009) 515.
[10] W.-S. Yoon, M. Balasubramanian, X.-Q. Yang, J. McBreen, J. Hanson, Electrochem. Solid-State Lett. 8 (2005) A83.
[11] W. Yoon, J. Hanson, J. Mcbreen, X. Yang, Electrochem. Commun. 8 (2006) 859.
[12] W.-S. Yoon, K.Y. Chung, M. Balasubramanian, J. Hanson, J. McBreen, X.-Q. Yang, J. Power Sources 163 (2006) 219.
[13] S.-H. Kang, P. Kempgens, S. Greenbaum, a. J. Kropf, K. Amine, M.M. Thackeray, J. Mater. Chem. 17 (2007) 2069.
[14] B.H. Toby, R.B. Von Dreele, J. Appl. Crystallogr. 46 (2013) 544.
[15] S.-H. Kang, C.S. Johnson, J.T. Vaughey, K. Amine, M.M. Thackeray, J. Electrochem. Soc. 153 (2006) A1186.
[16] Y. Hinuma, Y.S. Meng, K. Kang, G. Ceder, Chem. Mater. 19 (2007) 1790.
[17] A. Rougier, J. Electrochem. Soc. 143 (1996) 1168.
[18] Y. Gao, M. Yakovleva, W. Ebner, Electrochem. Solid-State Lett. 1 (1998) 117.
[19] J. Reed, G. Ceder, Chem. Rev. 104 (2004) 4513.
[20] H. Kim, D. Seo, I. Park, J. Hong, K.-Y. Park, K. Kang, Chem. Mater. 24 (2012) 720.
[21] H. Arai, S. Okada, Y. Sakurai, J. Yamaki, Solid State Ionics 109 (1998) 295.
[22] G.S. Pawley, J. Appl. Crystallogr. 14 (1981) 357.
[23] H. Yang, G.V. Zhuang, P.N. Ross, J. Power Sources 161 (2006) 573.
[24] E.-S. Hong, S. Okada, T. Sonoda, S. Gopukumar, J. Yamaki, J. Electrochem. Soc. 151 (2004) A1836.
[25] A. Boulineau, L. Croguennec, C. Delmas, F. Weill, Dalton Trans. 41 (2012) 1574.
[26] Y. Gao, Y. Liang, S.A. Chambers, Surf. Sci. 365 (1996) 638.